Supplementary Material for 'Multi-mode Bus Coupling Architecture of Superconducting Quantum Processor'

Changhao Zhao,[1,2] Yongcheng He,[1,2] Xiao Geng,[1,2] Kaiyong He,[1,2] Genting Dai,[1,2] Jianshe Liu,[1,2] and Wei Chen[1,2,3,∗]

[1]*Laboratory of Superconducting Quantum Information Processing,*
School of Integrated Circuits, Tsinghua University, Beijing 100084, China
[2]*Beijing National Research Center for Information Science and Technology, Beijing 100084, China*
[3]*Beijing Innovation Center for Future Chips, Tsinghua University, Beijing 100084, China*

S1. MODEL PARAMETERS

In our work, multi-mode coupling cQED systems are modeled with QuTiP and the parameters are determined based on common cQED experiments. In this section, we briefly describe how the parameters are determined in the simulations.

A. Qubit frequencies

Qubit frequencies are generally set below $8.00\,\mathrm{GHz}$, with enough qubit-resonator detuning to maintain dispersive coupling. The coupling frequencies $\omega^{(\mathrm{q})}/2\pi$ are around $7.70\,\mathrm{GHz}$. When both idle qubits and coupling qubits are included, idle frequencies $\omega^{(\mathrm{i})}/2\pi$ always lie below coupling frequencies $\omega^{(\mathrm{q})}/2\pi$, reaching the lowest level of $\sim 6.00\,\mathrm{GHz}$. Three-level transmon model is applied throughout our simulations. The anharmonicities for all qubits are $\alpha = -0.22\,\mathrm{GHz}$, which is expected to be unaltered in the frequency tuning range.

B. Bus coupler frequencies

The frequency of single-mode bus coupler is set at $\omega_1^{(\mathrm{r})}/2\pi = 8.00\,\mathrm{GHz}$, for whatever qubit coupling frequencies used. As for M-mode coupler, the mode frequency is determined so that the detuning $\omega^{(\mathrm{q})} - \omega_M^{(\mathrm{r})}$ is scaled by a factor of M and that it provides similar coupling strength J_M compared with the single-mode case. Therefore, definition of $\omega_M^{(\mathrm{r})}$ ($M = 1, 2, 3, \dots$) can be written as

$$\frac{\omega_1^{(\mathrm{r})}}{2\pi} = 8.00\,\mathrm{GHz},$$
$$\omega_M^{(\mathrm{r})} = \omega^{(\mathrm{q})} + M \times (\omega_1^{(\mathrm{r})} - \omega^{(\mathrm{q})}). \tag{S1}$$

It is noted here that the M-mode bus coupler frequency defined with Eq. (S1) means that the M modes all have identical frequencies. Practically, resonator mode frequencies always deviate from designed values and cannot be fabricated identical. To take these deviations into

account, for the simulations that correspond to Fig. 3(b) and Fig. 7 in the paper, randomized bus mode frequencies are applied, which are subject to a uniform distribution within $\pm 10\,\mathrm{MHz}$ range of the target frequency $\omega_M^{(\mathrm{r})}/2\pi$, Such simulations are executed repetitively (20 repetitions for Fig. 3(b) and $10 \sim 13$ repetitions for Fig. 7) to capture the average effects of multi-mode bus coupling. Except for these two sets of simulations, all the others use multi-mode bus couplers without randomization.

C. Coupling strengths

For any direct capacitive coupling between a qubit and a resonator mode, the coupling strength is fixed at $g^{(\mathrm{rq})}/2\pi = 30\,\mathrm{MHz}$. Together with the qubit and resonator frequencies defined above, it is guaranteed that the criterion of dispersive coupling approximation can be satisfied. Although $g^{(\mathrm{rq})}$ is actually dependent on qubit and resonator frequencies, this effect has been ignored in our simulations since it is only a minor variation within the frequency range involved.

D. Decoherence

For most of the simulations executed in this work, the system is assumed to be free from decoherence. The only simulations that involve decoherence is the Purcell effect simulations, which are demonstrated in Fig. 5 and Fig. 6 . In order to clearly demonstrate the impact of Purcell effect on qubit coherence, the bare energy relaxation rate and dephasing rate of the qubit are kept at zero, while each bus resonator mode is assigned high energy relaxation rate of $\kappa = 10\,\mathrm{MHz}$.

E. Initial states

Our simulation models generally contain two coupling qubits and M bus coupler modes. By default, the two qubits are initialized to $|q_1 q_2\rangle = |10\rangle$ and the bus modes are initialized to vacuum states. When idle qubits are included to investigate their residual XY coupling effects, each of them are initialized to $|+\rangle \equiv (|0\rangle + |1\rangle)/\sqrt{2}$ (see
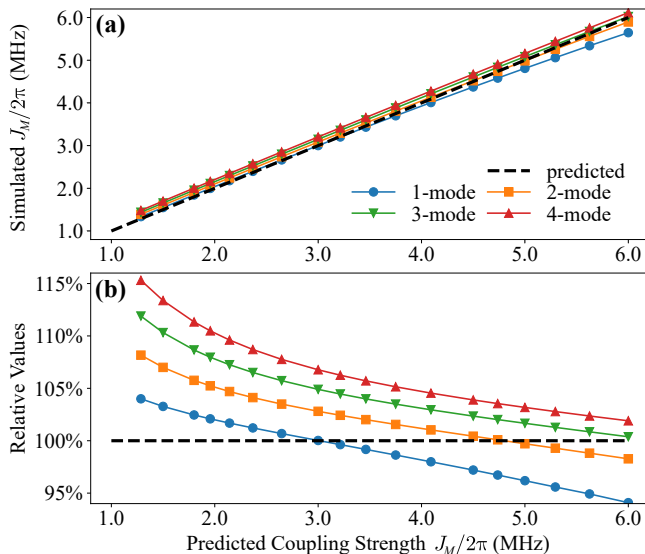
* weichen@mail.tsinghua.edu.cn

FIG. S1. Multi-mode virtual photon coupling strengths extracted from QuTiP simulations compared to predictions given by Eq. (4). Both (a) absolute magnitudes and (b) relative magnitudes of simulated values are demonstrated versus the predicted values.

Sec. S3). As for two-qubit quantum process tomography, it involves 16 two-qubit initial states from the set $\{|0\rangle, |1\rangle, |+\rangle, |\widetilde{+}\rangle\}^{\otimes 2}$, where $|\widetilde{+}\rangle \equiv (|0\rangle + \mathrm{i}|1\rangle)/\sqrt{2}$.

F. Time evolutions

Except for the calculation of residual ZZ coupling strength in Fig. 9, all simulations are executed by solving for system time evolutions with QuTiP method `mesolve()`. And except for the simulation of control pulse imperfections in Fig. 10, all time evolutions involve only static Hamiltonians without explicit time dependence. In such static-Hamiltonian simulations, iSWAP gate operation times t_{iSWAP} and virtual photon coupling strengths J_M (see Sec. S2) are obtained by fitting qubit population curves to cosine functions, and quantum process tomography of iSWAP gate are based on the expectation values of the observables (two-qubit direct products of Pauli operators) at $t = t_{\mathrm{iSWAP}}$.

S2. EXTRACTION OF SIMULATED J_M

As discussed in the paper, Eq. (4) provides a theoretical conjecture of multi-mode virtual photon coupling strength. On the other hand, t_{iSWAP} can be extracted from our simulations and $J_M = \pi/2t_{\mathrm{iSWAP}}$ are then calculated and compared to the predicted values of Eq. (4), as shown in Fig. S1. When J_M is weak (strong), i.e. the detuning between the qubit and the bus mode is relatively large (small), the theoretical values tend to be

lower (higher) than QuTiP simulation values. When J_M is about 2 MHz to 5 MHz, the predictions for $M = 1 \sim 4$ are within 10% error range of the QuTiP simulation results. Since Eq. (1) is used as the Hamiltonian of the QuTiP simulations, these errors can be attributed mainly to the dispersive coupling approximation process from Eq. (1) to Eq. (2), and also possibly to the extrapolation from Eq. (3) to Eq. (4). Although the errors may not be negligible in general, Eq. (4) still provides reasonable approximations of the effective inter-qubit coupling strengths in multi-mode bus coupling architecture.

S3. IDLE QUBITS IN RESIDUAL XY COUPLING SIMULATIONS

To study residual XY coupling effects among qubits, we add idle qubits to the simulated models. The QuTiP models contain two coupling qubits Q1 and Q2 at $\omega^{(\mathrm{q})}/2\pi = 7.70\,\mathrm{GHz}$ and the direct coupling strengths between the qubits and the bus coupler modes are fixed at $g^{(\mathrm{rq})}/2\pi = 30\,\mathrm{MHz}$. The frequencies of the bus modes are determined by Eq. (S1). Additionally, a number of idle qubits are included in the models. The idle qubits are off-resonance with Q1 and Q2, so that energy exchange between the coupling qubits and the idle qubits are suppressed. The direct coupling strengths between the idle qubits and the bus resonator modes are also fixed at $g^{(\mathrm{rq})}/2\pi = 30\,\mathrm{MHz}$. The number of idle qubits as well as their idle frequencies and initial states

$$|\psi_0^{(\mathrm{i})}(\theta_0, \phi_0)\rangle = \cos(\theta_0/2)|0\rangle + \exp(\mathrm{i}\phi_0)\sin(\theta_0/2)|1\rangle \ \ (\mathrm{S2})$$

can be varied in different simulations. It is assumed that all qubits and bus resonator modes suffer no decoherence effects, so the system evolution follows Schrödinger equation or von Neumann equation.

Our first idle qubit simulation involves one idle qubit I1 at $\omega^{(\mathrm{i})}/2\pi = 7.64\,\mathrm{GHz}$, which is insufficiently detuned from the coupling qubits at $\omega^{(\mathrm{q})}/2\pi = 7.70\,\mathrm{GHz}$ so that the unintended XY coupling can be easily identified. A single-mode resonator R1 at $8.00\,\mathrm{GHz}$ is used as the bus coupler. The initial state of the idle qubit is given in the form of Eq. (S2) with a fixed $\phi_0 = 0$ (simulations suggest that ϕ_0 does not affect residual XY coupling) and a varied $\theta_0 = s \times \pi/8$ ($s = 0, 1, \ldots, 8$). Solving Schrödinger equation for the system time evolution from $0\,\mu\mathrm{s}$ to $4\,\mu\mathrm{s}$ yields the results shown in Fig. S2.

In Fig. S2, the red curves represent the evolution of I1. Since current model is assumed free of decoherence, the average population of I1 is generally stable at its initial value. The blue curves represent the evolution of R1, which is generally stable at vacuum state as expected. The rapidly oscillating orange and green curves represent the evolution of Q1 and Q2. When I1 starts in its energy eigen state $|0\rangle$ or $|1\rangle$ as shown in Fig. S2(e)(i), the coherent state swap processes of Q1 and Q2 are stable. However, when I1 starts in some superposition state,
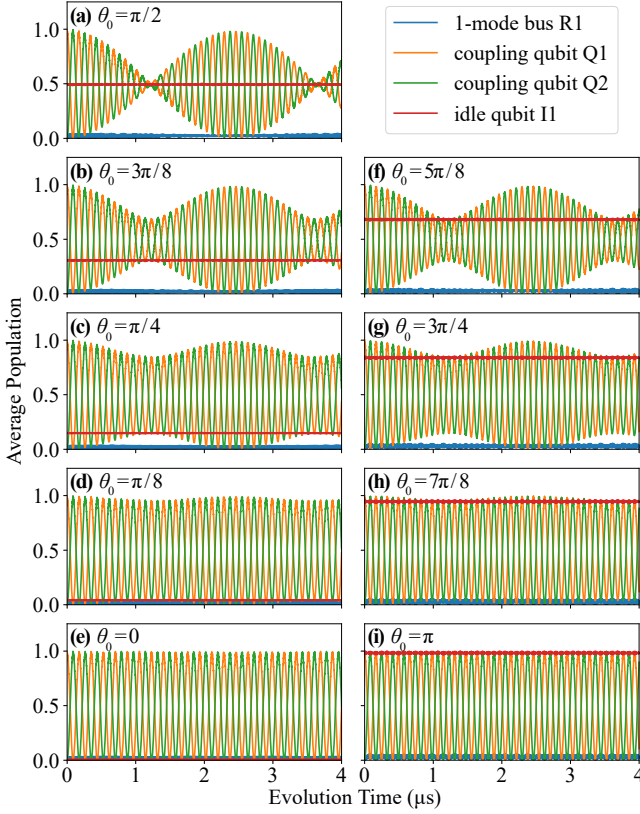
FIG. S2. Residual XY coupling from the idle qubit affecting the state swap process of the two coupling qubits. When the idle qubit is initialized to some superposition state $(0 < \theta_0 < \pi)$, the state swap amplitudes are modulated periodically. When the idle qubit is initialized to its eigen state $(\theta_0 = 0, \pi)$, the state swap amplitudes are unaffected.

Q1-Q2 state swap process appears to be modulated periodically in amplitude and the modulation valleys coincide with the average population of I1. Specially, when I1 is initialized to $|\psi_0^{(i)}\rangle = (|0\rangle + |1\rangle)/\sqrt{2} \equiv |+\rangle$, i.e. $\theta_0 = \pi/2$ as shown in Fig. S2(a), Q1-Q2 state swap amplitude will decrease to zero and then revive to maximum. Comparison of all the subfigures suggests that if the idle qubit is closer to its eigen state, it interferes less with the coupling qubits. Nevertheless, the periods of amplitude modulations are identical for different initial states of the idle qubit. Therefore the amplitude modulation period of the state swap process is a proper figure of merit to characterize residual XY coupling strengths in bus coupling architecture and we can fix the idle qubit initial state at $|+\rangle$ to best manifest residual XY coupling effects in following simulations.

Fig. S3 depicts how systems with different numbers of idle qubits evolve within 50 μs. The orange curves represent the population of the coupling qubits Q1 and Q2. Since the total evolution time is much longer than one cycle of Q1-Q2 state swap, details of the process are not visible in the figure, yet the envelopes of Q1 and Q2 pop-
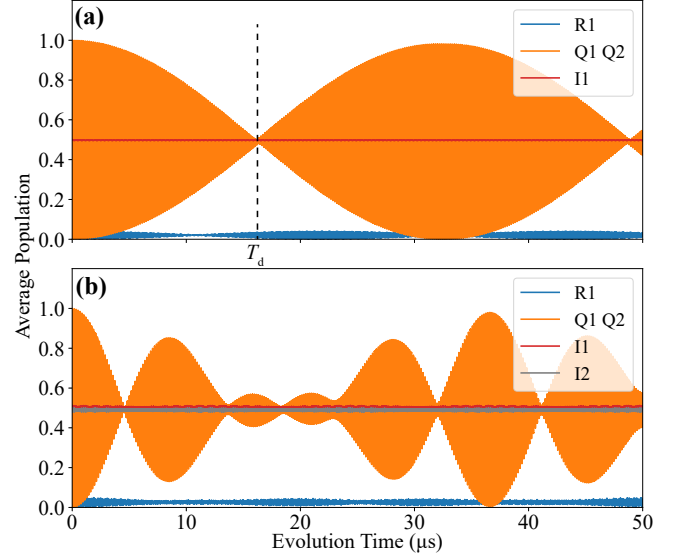

FIG. S3. Residual XY coupling from varied number of idle qubits. (a) Single idle qubit I1 at 7.40 GHz, posing a cosine modulation on the state swap process of Q1 and Q2. (b) Two idle qubits I1 and I2 at 7.40 GHz and 7.50 GHz, posing double cosine modulation on the state swap process of Q1 and Q2.

ulation curves clearly reflect the coupling from the idle qubits. Fig. S3(a) corresponds to a single idle qubit I1 at $\omega_1^{(i)}/2\pi = 7.40$ GHz. It can be seen that Q1-Q2 population curve is modulated by a cosine envelope. Fig. S3(b) corresponds to two idle qubits I1 and I2, whose idle frequencies are $\omega_1^{(i)}/2\pi = 7.40$ GHz and $\omega_2^{(i)}/2\pi = 7.55$ GHz respectively. In this case, Q1-Q2 population curve is double modulated by two cosine envelopes of different modulation periods. The long-period envelope induced by I1 is superposed by the short-period envelope induced by I2, which indicates that idle qubits closer in frequency to the coupling qubits would introduce stronger coupling. Although bus coupling architecture usually contains multiple idle qubits, we can focus on the one that is closest in frequency to the coupling qubits to analyze residual XY coupling effects.

It is addressed here that residual XY coupling is basically the result of the effective virtual photon coupling provided by the bus coupler and that high-order perturbation effects of the bus coupler do not necessarily engage. Then the QuTiP model may exclude the bus resonator modes and adopt the theoretical virtual photon coupling strength J_M in Eq. (4) as the approximated direct coupling strength between different qubits, leading to 'pseudo-bus Hamiltonian'

$$\frac{\hat{H}_{\text{pseudo}}}{\hbar} \approx \sum_k \left(\omega_k^{(q)} \hat{b}_k^\dagger \hat{b}_k + \frac{\alpha_k}{2} \hat{b}_k^\dagger \hat{b}_k^\dagger \hat{b}_k \hat{b}_k \right) + \sum_{k \neq l} J_{M(kl)} (\hat{b}_k^\dagger \hat{b}_l + \hat{b}_k \hat{b}_l^\dagger). \tag{S3}$$

The validity of this simplification is supported by the

results in Fig. S1 that Eq. (4) gives reasonable approximations of the virtual photon coupling strengths. Since a model with more than a few qubits and resonators would be exceedingly time-consuming for QuTiP simulation, such simplification enables efficient analysis of multi-mode bus coupling systems that accommodate more qubits and is applied in the simulations from which 'distortion times' are extracted (See Fig. 8 in the paper).

S4. RESIDUAL ZZ COUPLING STRENGTH

According to Ref. [1], when a single-mode bus resonator couples two three-level transmons, fourth-order perturbation results for residual ZZ coupling strength

can be written as

$$
\zeta_{\text{pert}} = -2 \left(g_1^{(\text{rq})} g_2^{(\text{rq})} \right)^2 \\
\times \left(\frac{1}{\delta_1 \Delta_1^2} + \frac{1}{\delta_2 \Delta_2^2} + \frac{1}{\Delta_1 \Delta_2^2} + \frac{1}{\Delta_2 \Delta_1^2} \right). \tag{S4}
$$

$\Delta_k \equiv \omega_k^{(\text{q})} - \omega^{(\text{r})}$ is the detuning between qubit k ($k = 1, 2$) and the bus mode. $\delta_1 \equiv \omega_2^{(\text{q})} - (\omega_1^{(\text{q})} + \alpha_1)$ and $\delta_2 \equiv \omega_1^{(\text{q})} - (\omega_2^{(\text{q})} + \alpha_2)$ are the detunings between 0-1 energy level spacing of one qubit and 1-2 energy level spacing of the other.

Similar to the extrapolation from J_1 to J_M (see Eq. (4) in the paper), we make a wild guess for residual ZZ coupling strength in multi-mode coupling architecture as

$$
\zeta_{\text{pert}} = \sum_{m=1}^{M} \zeta_{\text{pert}}^{(m)}, \tag{S5}
$$

where $\zeta_{\text{pert}}^{(m)}$ denotes the residual ZZ coupling strength provided by the m-th bus coupler mode. Eq. (S5) has been used in Fig. 10 for calculation of the perturbative results of multi-mode coupling (dashed curves).

[1] L. Dicarlo, J. M. Chow, J. M. Gambetta, L. S. Bishop, B. Johnson, D. Schuster, J. Majer, A. Blais, L. Frunzio, S. M. Girvin, *et al.*, Demonstration of two-qubit algo- rithms with a superconducting quantum processor, Nature **460**, 240 (2009).